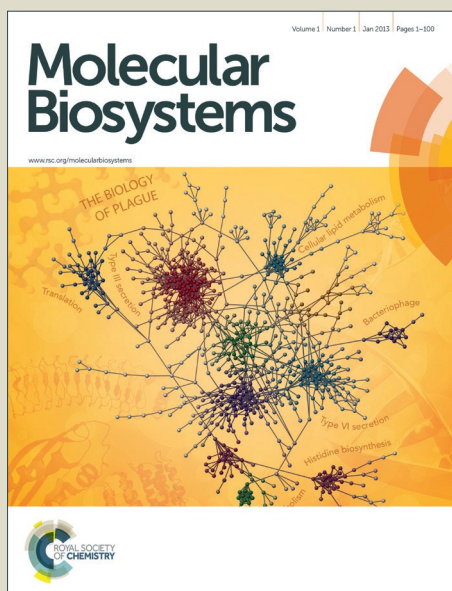


Molecular BioSystems

Accepted Manuscript



This article can be cited before page numbers have been issued, to do this please use: C. Chang, S. Jeyachandran, N. Hu, C. Liu, S. Lin, Y. Wang, Y. Chang and M. Hou, *Mol. BioSyst.*, 2015, DOI: 10.1039/C5MB00582E.



This is an *Accepted Manuscript*, which has been through the Royal Society of Chemistry peer review process and has been accepted for publication.

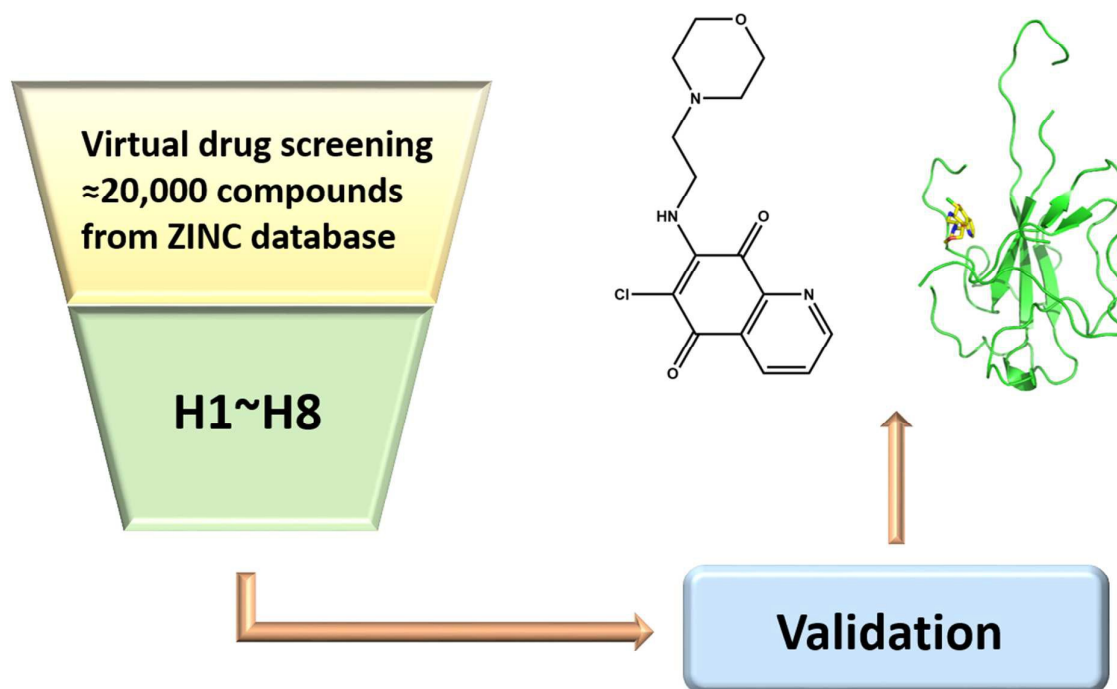
Accepted Manuscripts are published online shortly after acceptance, before technical editing, formatting and proof reading. Using this free service, authors can make their results available to the community, in citable form, before we publish the edited article. We will replace this *Accepted Manuscript* with the edited and formatted *Advance Article* as soon as it is available.

You can find more information about *Accepted Manuscripts* in the [Information for Authors](#).

Please note that technical editing may introduce minor changes to the text and/or graphics, which may alter content. The journal's standard [Terms & Conditions](#) and the [Ethical guidelines](#) still apply. In no event shall the Royal Society of Chemistry be held responsible for any errors or omissions in this *Accepted Manuscript* or any consequences arising from the use of any information it contains.

Structure-based virtual screening and experimental validations for discovery of inhibitors targeted towards the human coronavirus nucleocapsid protein

Graphical Abstract



Structure-based virtual screening and experimental validations for discovery of inhibitors targeted towards the human coronavirus nucleocapsid protein

Chung-ke Chang^{1§}, Sivakamavalli Jeyachandran^{2§}, Nien-Jen Hu^{3§}, Chia-Ling Liu^{2§}, Shing-Yen Lin², Yong-Sheng Wang², Yu-Ming Chang⁴, and Ming-Hon Hou^{2,3*}

¹*Institute of Biomedical Science, Academia Sinica, Nangang, Taipei, Taiwan*

²*Institute of Genomics and Bioinformatics and Institute of Life Sciences, National Chung Hsing University, Taichung 40254, Taiwan*

³*Institute of Biochemistry, National Chung Hsing University, Taichung 40254, Taiwan*

⁴*Institute of Biological Chemistry, Academia Sinica, Taipei 11529, Taiwan*

§These authors contributed equally to this work.

Corresponding Authors:

*Author to whom correspondence should be addressed; E-Mail: mhho@nchu.edu.tw; Tel.: +886-4-2284-0338 (ext. 7011); Fax: +886-4-2285-9329.

Nucleocapsid protein (NP), an essential RNA-binding viral protein in human coronavirus (CoV)-infected cells, is required for the replication and transcription of viral RNA. Recent studies suggested that human CoV NP is a valid target for antiviral drug development. Based on this aspect, a structure-based virtual screening approach to targeting nucleocapsid protein (NP) was performed to identify good chemical starting points for medicinal chemistry. The present study utilized structure-based virtual screening against Human CoV-OC43 using the Zinc database, which is performed through docking with varying precisions and computational intensities to identify eight potential compounds. The chosen potential leads were further validated experimentally using biophysical means. Surface plasmon resonance (SPR) analysis indicated that one among the potential leads, 6-Chloro-7-(2-morpholin-4-yl-ethylamino) quinoxaline-5, 8-dione (small-compound H3), exhibited a significant decrease of RNA-binding capacity of NP by more than 20 %. The loss of binding activity was manifested as a 20% decrease in the minimum on-rate accompanied with a 70% increase in the maximum off-rate. Fluorescence titration and X-ray crystallography studies indicated that H3 antagonizes the binding between HCoV-OC43 NP and RNA by interacting with the N-terminal domain of the NP. Our findings provide insight into the development of new therapeutics, which disrupts the interaction between RNA and viral NP in the HCoV. The discovery of the new compound would be an impetus to design novel NP inhibitors against human CoV.

Keywords: Coronaviruses, Nucleocapsid protein, N-terminal domain, Surface Plasmon Resonance, X-ray crystallography, RNA-binding inhibition, Nucleocapsid protein inhibitor.

Data deposition:

The atomic coordinates and structure factors for OC43 complexes with H3 (4LMT) have been deposited in the RCSB Protein Data Bank.

Introduction

Respiratory tract infection (RTI) is one of the infectious diseases causing serious mortality among young children and adults in developing countries¹⁻³. Most of the RTI diseases are caused by the RNA viruses, including respiratory syncytial virus (RSV), influenza viruses, rhinoviruses, parainfluenza viruses, human metapneumovirus and human coronaviruses (HCoVs)⁴⁻⁸. Coronaviruses (CoVs) are positive strand, enveloped RNA viruses with genome sizes ranging from 27–33 kilobases (kb) and belong to the Coronaviridae family. Its classification includes α -, β -, γ - and δ -coronaviruses⁹. HCoV-NL63 and HCoV-229E belong to the α -coronaviruses while HCoV-OC43, HCoV-HKU1, and the severe acute respiratory syndrome coronavirus (SARS-CoV) belong to the β -coronaviruses⁹. The pathogen Middle East Respiratory Syndrome coronavirus (MERS-CoV) belongs to the genus β -coronavirus¹⁰.

Due to the severe pathogenic capability, e.g. Severe Acute Respiratory Syndrome (SARS) pandemic in Asia during 2003-2004 and the recent outbreak of Middle-East Respiratory Syndrome (MERS), and their dreadful nature, human coronaviruses have attracted clinical interests, recently^{11, 12,13}. Moreover, there are no efficacious therapies against coronaviral diseases so far, promoting the development of anti-coronavirus compounds. CoVs are composed of several structural proteins sharing high conservation across species: the small envelope (E) protein, matrix (M) glycoprotein, the trimeric spike (S) glycoprotein bound to the viral membrane, and the nucleocapsid protein (NP) residing inside the virus. Some variants contain a third membrane-bound glycoprotein, HE (hemagglutinin-esterase)¹⁴. The nucleocapsid protein (NP) is one of the most abundant structural proteins in CoVs, and serves multiple functions, such as ribonucleoprotein formation, modulation of host cell metabolism, and regulation of viral RNA synthesis during replication and transcription^{15,16}.

In addition, coronavirus NPs consist of 3 domains: an N-terminal RNA-binding domain (NTD), an intrinsically disordered central Ser/Arg (SR)-rich linker that may contain the protein's primary phosphorylation sites, and a C-terminal dimerisation domain (CTD). Crystal structures of several coronavirus NP-NTDs have been determined previously, including those encoded by infectious bronchitis virus (IBV), mouse hepatitis virus (MHV), HCoV-OC43, and SARS-CoV.¹⁷⁻²² Furthermore, crystal structures of CoV NPs-CTDs provide structural clues on how the building blocks for coronavirus nucleocapsid form through NP dimer^{17-19, 22-25}. Because of their importance in the viral life cycle, NPs are becoming the unique targets for therapeutic development against the viral diseases¹⁶. Two strategies to inhibit oligomeric NP function have been reported²⁶. The first is to enhance or inhibit its oligomerization properties²⁷. The second strategy is to disrupt the RNA-binding site²⁸. We have previously identified a unique ribonucleotide-binding pocket consisting of highly conserved residues in the centre of NTD by solving the complex structure of CoV NP-NTD bound with a ribonucleotide monophosphate. Compounds binding to this RNA-binding pocket may inhibit normal NP function and could be used to combat CoV diseases²⁸.

Recently, this problematic research has attracted particular interest in virology due to the demand for new antivirals, preferably with a completely different mechanism of action from traditional antiviral drugs to avoid resistance and cross-resistance. The interaction between HCoV NP and RNA is an optimal target for CoV drug design. The strategy would be helpful to find out new potential leads to disrupt the functions of HCoV NP. In this paper we utilized the crystal structure of HCoV NPs NTD domain²⁷ as the target of a virtual screening endeavor using LIBDOCK. Eight potential leads (H1~H8) were initially selected targeting the active site of HCoV NPs. We further studied the effects of the eight compounds on the RNA-binding affinity

of NP by SPR experiments. Among the 8 leads, 6-Chloro-7-(2-morpholin-4-yl-ethylamino) quinoxaline-5, 8-dione (H3), revealed inhibition activity on the RNA-binding of NP. Crystal structure of HCoV-OC43 NP-NTD in complex with H3 was also determined depicting the detailed binding interactions. Our findings provide new insights into the development of novel drugs that may disrupt the interaction between RNA and viral NPs in HCoVs.

Materials and Methods

Protein preparation

Expression and purification of the NTD of HCoV-OC43 NP were performed as previously described²⁷. The purified protein was concentrated with an Amicon Ultra-15 centrifugal filter unit (Millipore, MA, USA) with a molecular weight cut-off of 3 kDa and stored at -80 °C. The Bradford method was used to determine protein concentrations using Bio-Rad protein assay reagents (Bio-Rad, CA, USA).

Structure-based virtual screening

Ligand screening and molecular docking were performed with the LIBDOCK module in Discovery Studio, version 2.5 (DS 2.5). The publicly available ZINC database version 12 was

chosen for virtual screening. The database was initially filtered to remove unreasonable molecules with unwanted physical and chemical properties. Molecules with the following properties were removed by default: molecular weight >600, log P < -4, log P > 8, hydrogen bond donors and acceptors >12, rotatable bonds >10, polar surface area >140, single bond chain length >6, chiral centers >4, unconstrained chiral centers >3, transition metals >8 rings, and d-hybrids. After filtering, the selected molecules comprised of over 20,000 compounds from several drug databanks in the ZINC database were utilized to generate multiple conformations using the conformation search and minimization program in DS 2.5. The final 3D multiple conformations database was subjected to the pharmacophore query. The LIBDOCK molecular docking software was used to screen for small molecules that may bind to a structure of the NTD of HCoV-OC43 NP using default parameters. The binding pocket of the NTD, which includes Tyr124, Tyr126, Arg122, and Arg164, were represented by a set of spheres during the docking process. It produces protein–ligand complexes and each conformer was simultaneously subjected to side chain and backbone refinements. The conformers were ranked within 30 kcal/mol of the minimum energy using the energy minimization module. The screened conformers were passed to a final round of docking and scoring. The non-bonding interactions between the inhibitors and the receptor proteins were displayed in Pymol. The 8 potential hits were identified by looking for interaction characteristics (e.g. π - π stacking interactions) between HCoV-OC43 NP-NTD and hit compounds which closely mimic the ones between HCoV-OC43 NP-NTD and ribonucleotide.

SDS-PAGE analysis

Polyacrylamide gel electrophoresis (12%) was performed on eluted fractions under reducing (β -mercaptoethanol) and non-reducing conditions²⁹. After electrophoresis, the gel was stained

with Coomassie brilliant blue (BioShop, Taiwan). The molecular mass of the purified HCoV-OC43 NP-NTD was determined by comparison of its electrophoretic mobility with those of molecular mass marker proteins (GeneDireX, Taiwan). The homogeneity and molecular mass of the HCoV-OC43 NP-NTD were also confirmed by gel filtration on a FPLC column (GE Healthcare Bio-Sciences, Taiwan). Total protein concentration was determined by the Bradford method²¹ using bovine serum albumin (BSA) as a standard.

Crystallization and data collection

Crystals of HCoV-OC43 NP-NTD-H3 complexes were obtained by co-crystallization using an HCoV-OC43 NP-NTD solution (8 mg/ml) pre-incubated for 30 min with H3. High-quality crystals suitable for X-ray diffraction were grown by standing a reservoir solution containing 30% (v/v) glycerol as cryo-protectant at room temperature for 2 days²⁷. Crystals were flash cooled under a nitrogen-gas stream at 100 K. X-ray diffraction data for the HCoV-OC43 NP-NTD were collected at the BL13B1 beam line of the National Synchrotron Radiation Research Center (NSRRC, Hsinchu, Taiwan)²⁸. All diffraction images were recorded using an ADSD Q315 CCD detector, and the data were processed and scaled using the HKL2000 software package³⁰. Data collection statistics are summarized in **Table 2**.

Structure determination and refinement

Because the new crystals grown in this study were isomorphous to those from HCoV-OC43 NP-NTD solved previously, the structures of the HCoV-OC43 NP-NTD complexes were determined using the structure of HCoV-OC43 NP-NTD (PDB ID:3V3P) as a base²⁷. For each structure, iterative cycles of model building with Mifit and computational refinement with CNS

were performed; 5% reflections were set aside for R_{free} calculations^{30, 28}. The stereochemical quality of the structures was assessed with the program *PROCHECK*²⁸. The molecular figures were produced with PyMOL (Shroedinger LLC, <http://www.pymol.org>).

Surface plasmon resonance (SPR) binding experiments

A BIAcore 3000A SPR instrument (Pharmacia, Uppsala, Sweden) equipped with a SA5 sensor chip (Pharmacia) was used to obtain the association and dissociation rate constants between HCoV-OC43 NPs and RNA. The repeated intergenic sequence of HCoV-OC43, 5'-biotin-(UCUAAAC)₄-3', was used as a probe in our SPR experiments. Experiments were conducted by injecting NP in 50 mM Tris (pH 7.5) with 150 mM NaCl and 0.1% CHAPS in the presence and absence of the H3 compound. The sensorgrams were fit to the 1:1 Langmuir model using the BIA evaluation software (version 3) to determine the association and dissociation rate constants (k_a , k_d)³¹. Binding affinities were calculated from the rate constants within the software. The chip surface was then washed with 10 μ l of 10 mM HCl to eliminate non-specific binding. The second flow cell was unmodified and served as a control. A blank buffer solution was then passed over the chip to initiate the dissociation reaction; this step was continued for an additional 600 s until the reaction was complete. After 600 s, the surface was recovered by washing with 10 μ l of 0.1% SDS for each single-stranded RNA. Before fitting to the 1:1 Langmuir model, the binding data were corrected by subtracting the control to account for refractive index differences.

Fluorescence spectroscopy

Experiments were conducted in buffer consisted of 50 mM Tris (pH 7.3), 100 mM NaCl, and 0.1% CHAPS. Tryptophan fluorescence was measured at 330 nm with a Hitachi F-4500

fluorescence spectrophotometer using an excitation wavelength of 288 nm and a 1-cm light path. Emission data were also collected for wavelengths ranging from 300 to 400 nm. Three repeats were recorded for all static measurements. The relative fluorescence change intensity was determined using the following equation: $\text{Change \%} = (\text{FL}_{\text{NP}} - \text{FL}_{\text{NP-drug}}) / \text{FL}_{\text{NP}} * 100$, where FL_{NP} is the NP fluorescence in the absence of compound, and $\text{FL}_{\text{NP-drug}}$ is the fluorescence of the NP-compound complex³². In the fluorescence titration assay, a final concentration of 4 μM HCoV-OC43 NP was added to different concentrations of compound, and the samples were incubated at 4°C for various durations. The binding constant between H3 and NP was obtained by fitting the average of H3-induced fluorescence changes (ΔF) from three separate experiments at 3 h following the addition of test compounds as previously described²⁸.

Results and discussion

The effects of 6-chloro-7-(2-morpholin-4-yl-ethylamino) quinoxaline-5,8-dione (H3) on RNA binding activity of NP.

Several potential hits, H1~H8 were identified with high docking score for the distinct ribonucleotide-binding pocket with conserved residues (Arg 122, Tyr 124, Tyr 126, and Arg 164) (**Figure 1A and 1B**), using a molecular docking software (LIBDOCK) described in the Materials and Methods section. The RNA-binding capacities of HCoV-OC43 NP-NTD in the presence of these eight compounds were further studied by surface plasmon resonance (SPR). Only treatment with 6-chloro-7-(2-morpholin-4-yl-ethylamino) quinoxaline-5, 8-dione (**Compound H3, Table S2 and Figure 2A**) produced significant decrease of RNA-binding capacity of NP by more than 20 %. Interestingly, H3 is a potent inhibitor of CDC25 protein phosphatases, exhibiting marked anti-proliferative activity against human MCF-7 breast cancer cells²⁹ and arrest of synchronized cells in both the G1 and G2/M phases¹⁹. Adding H3 in the assay resulted in a loss of binding capacity of NP to the RNA as evidenced by the decrease in response units **RU (Figure 2B)**, suggesting that H3 hinders the binding of HCoV-OC43 NP to RNA. The loss of binding activity manifested as a 20% decrease in the minimum on-rate accompanied by a 70% increase in the maximum off-rate (**Figure 2C and Table 1**).

We have shown that H3 interferes with the binding activity between HCoV-OC43 NPs and RNA, raising the possibility that H3 may also interact directly with the HCoV-OC43 NP. Thus, we tested this possibility using a fluorescence titration assay by scanning the fluorescence emission spectra of NP between 300-400 nm in the presence and absence of 2 μ M H3 (**Figure 3A**). The wavelength with maximal emission was determined to be at approximately 331 nm in both the presence and absence of H3, indicating that the interaction between H3 and NP did not

noticeably shift the emission spectrum. To exclude the possibility that the change of NP fluorescence caused by H3 was due to an inner filter effect, we measured the absorption spectra from 330~400 nm for H3 at different concentrations and no significant absorbance was observed up to 5 μ M H3 (**Figure S1**). Intriguingly, fluorescence titration assay showed that increasing drug concentration led to quenching of NP fluorescence (**Figure 3B**), suggesting that NP interacts specifically with H3. Assuming that the amount of changed fluorescence corresponds to the fraction of NP bound to H3, fitting of the binding curve (**Figure 3B**) resulted in an unambiguous 1:1 stoichiometry for the interaction between H3 and HCoV-OC43 NP with a K_d of 2.08×10^{-6} M. Together with the SPR results, our data indicate that H3 inhibits the RNA-binding activity of HCoV-OC43 NP by directly interacting with the NP protein.

Structure of the HCoV-OC43 NC-NTD complex with H3

To elucidate the molecular mechanism behind the binding between H3 and HCoV-OC43 NP, NP-NTD crystals were co-crystallized with H3 as described in the Materials and Methods section. The structure of the HCoV-OC43 NP-NTD in complex with H3 was determined by the molecular replacement using the crystal structure of the apo-HCoV-OC43 NP-NTD (PDB ID: 3V3P) as the search model. The final protein structure (**Figure 4A**) was refined to *R*-factor and *R*-free values of 0.221 and 0.232, respectively, at a resolution of 2.55 Å. A five-stranded anti-parallel β sheets sandwiched between loops (or short 3_{10} helix) form the core of HCoV-OC43 NP-NTD-H3 complex (**Figure 4A and 4B**). The complex structure is shaped like a right-handed fist, in which the palm and finger regions are rich in basic residues and the β -sheet core is flanked by the flexible loops¹¹. Residues 105 to 120 form a long flexible loop that protrudes out of the core and connects strands β 2 and β 3. The loop has poor electron density

probably due to its unstructured nature, making it relatively difficult to assign precise positions of the loop residues, especially for residues 115-117. The overall structure of the HCoV-OC43 NP-NTD-H3 complex is similar to that of apo-HCoV-OC43 NP-NTD (RMSD?), with a H3 molecule inserted into a cavity in the nucleotide-binding site of NP-NTD (**Figure 4B**).

The H3-binding pocket of nucleocapsid N-terminal domains

The H3-binding site is close to a positively charged patch which has been proposed to interact with the phosphate backbone of RNA¹⁷. The H3-binding site has well-defined electron density (**Figure 4C**), allowing a detailed analysis of the interactions between H3 and HCoV-OC43 NP-NTD (**Figure 4D**). The quinoline-5,8-dione ring forms a direct hydrogen bond to the Arg164 guanidinium group and a water-mediated hydrogen bond to the backbone carbonyl group of Phe66. The oxygen atom in the H3 morpholine ring forms another hydrogen bond with the Ala171 backbone amide. Tyr124 is located on the surface of HCoV-OC43 NP-NTD and interacts directly with the quinolone group present in H3. In addition, an anion- π interaction was observed between Phe57 and the oxygen atom of the quinoxaline moiety. The side chains of Phe66, Tyr124, Arg164, Phe57 and Arg171 generate a distinct binding pocket for the interaction with H3 via hydrogen bonding, anion- π and π - π stacking forces (**Figure 4E**). The specific interaction between Tyr124 and quinolone ring of H3 was also observed in the molecular docking results, further suggesting the validity of our virtual screening approach. However, the branched moiety is pointing towards the opposite side in the docking results. Compared to a previously identified coronavirus NP inhibitor, N-(6-oxo-5,6-dihydrophenanthridin-2-yl)(N,N-dimethylamino)acetamide hydrochloride (PJ34)¹⁹, both compounds utilize a polycyclic aromatic core to interact with Phe66 and Tyr124 of NP

through π - π stacking. However, the morpholin moiety of H3 and the branched moiety of PJ34 point towards opposite directions (**Figure 4F**), with the orientation of H3 closely resembling that of the natural substrate AMP when bound to NP-NTD (**Figure S2**).

Several studies have reported that the N-terminus of the SARS-CoV NP provides a scaffold for RNA binding^{25, 33}. X-ray crystallographies have also revealed a high degree of conservation among structural folds of NP-NTDs from various CoVs. The N-terminal region of IBV NP assists in the formation of the ribonucleocapsid via a lure and lock mechanism by facilitating long-range, non-specific interactions between the NP and viral RNA¹⁹. Multiple RNA binding sites on the NP of SARS-CoV have been identified that may bind to RNA cooperatively³⁴. Similar to the N-terminal domain of SARS-CoV and IBV NPs, the N-terminal domain of the HCoV-OC43 NP may also bind to RNA. In addition to the N-terminal domain, the highly positively charged central linker region was also capable of binding to RNA, whereas the C-terminal domain of the HCoV-OC43 NP did not show RNA-binding activity³⁴. As such, identification of compounds that bind to the N-terminal domain and interfere with NP-RNA interactions may provide valuable leads into development of broad-spectrum anti-coronaviral therapeutics. Several residues in NP-NTDs are critical for RNA binding and virus infectivity. We have previously shown that compounds binding to a unique RNA-binding pocket located in the center of CoV NP-NTD may be employed to combat pathogenic CoVs²⁸.

In this study, docking results suggest that several hits can bind to this ribonucleotide-binding pocket of CoV NP-NTD. Based on the SPR assay of NPs, we identified one potential compound that interferes RNA binding of CoV NP. Previously, we identified another CoV NP inhibitor, PJ34, using virtual screening²⁸. The higher resemblance between H3 and AMP

compared to that between PJ34 and AMP may explain the higher inhibitory effect of H3 towards the RNA-binding activity of HCoV-OC43 NP at the same protein-to-compound ratios (**Figure S2**). Interestingly, PJ34 (Compound H5) induced less fluorescence quenching compared to H3 (**Figure 1B**), which suggests that the extent of change induced by compounds may correlate with their relative inhibitory activity.

Conclusion

In summary, we identified a new NP inhibitor obtained from *in silico* virtual screening against CoV NPs and results were further verified experimentally with the SPR assay and X-ray crystallography. We also characterized the binding affinity of the compound with CoV NP by fluorescence studies suggesting small compound H3 as an effective inhibitor for the RNA-binding activity of CoV NPs. The development of novel NP-targeting agents are crucial for treating pathogenic HCoV infections and persistence of latent infection – problems that have been highlighted in the field of influenza and AIDS research. This study may assist the development of anti-viral drugs against HCoV. Based on this aspect, our findings will help explore the role of CoV NPs in ribonucleoprotein formation, metabolism and its multi-functional role in the eukaryotic system.

Conflict of Interest

None

Acknowledgments

This work was supported by NSC grant (103-2113-M-005 -007 -MY3) (M.-H. H). We would like to thank National Synchrotron Radiation Research Center (Taiwan) for X-ray data collection.

Figure legends

Figure 1. (A) Crystal structural of the HCoV-OC43 NP-NTD. The four conserved residues including Arg122, Tyr124, Tyr126, and Arg164 that contribute to the RNA binding at NP-NTD are marked (left). Surface representation of the the HCoV-OC43 NP-NTD: electrostatic potentials are colored in blue (positive) and red (negative) (right). **(B)** Amino acid sequence alignment, performed using T-coffee, of N-NTDs from HCoV-OC43, HCoV-HKU1, HCoV-229E, HCoV-NL63, SARS-CoV, MERS, IBV and MHV, all of which were retrieved from GenBank. Conserved residues including Arg122, Tyr124, Tyr126, and Arg164 is indicated with an asterisk.

Figure 2. (A) Chemical structure of H3 (NSC663284). **(B)** Sensorgram of the interaction between the immobilized single-stranded RNA and full-length HCoV-OC43 NPs in the presence of H3 at 2 μM . **(C)** Sensorgram of the interaction between the immobilized single-stranded RNA and full-length HCoV-OC43 NPs at various concentrations in the presence of H3.

Figure 3. (A) FL spectra of the NP (4 μM) incubated in the presence of H3 at various concentrations for 3 h; H3 was buffered with 20 mM Tris-HCl (pH 7.5) and 100 mM NaCl. **(B)** Nonlinear regression analyses of the relative fluorescence intensity change of the NP in the presence of various concentrations of H3 at various time points.

Figure 4. Structural overview of the HCoV-OC43 NP-NTD–H3 complex. **(A)** Ribbon representation of HCoV-OC43 NP-NTD with H3 depicted as a stick structure. **(B)** Electrostatic surface of the OC43 NP-NTD–H3 complex. Blue denotes positive charge potential, while red indicates negative charge potential. **(C)** 2Fo-Fc electron density map of H3 contoured at 1σ .

(D) Detailed stereoview of the interactions at the H3-binding site. The H3 molecule binds to this site via Ser64, Phe66, His104, Tyr124, and Tyr126. The dotted green lines denote hydrogen bonds. The red dashed lines indicate van der Waals interactions. **(E)** Schematic diagram of H3 bound to HCoV-OC43 NP-NTD. The hydrogen-bonding interactions mediated by the side- and main-chain atoms are marked as dot red and black lines, respectively. The anion- π interactions mediated by the side-chain atoms are denoted as blue dashed lines. The stacking interactions mediated by the side-chain atoms are marked as dashed green lines. **(F)** Structural superimposition of the native HCoV-OC43 NP-NTD (blue), HCoV-OC43 NP-NTD-H3 (green) and HCoV-OC43 NP-NTD-PJ34 (red) at the residues involved in ligand binding.

Table 1. The kinetic analysis of the SPR experiments examining binding of HCoV-OC43 nucleocapsid (N) proteins to RNA in the presence of H3.

sample	$k_d(S^{-1}M^{-1} \times 10^{-4})$	$k_a(S^{-1} \times 10^4)$	$K_D(nM)$	BC(RU)
NP	5.56	4.81	11.55	150
NP+H3	6.49	3.76	17.3	116

Table 2. Data collection and refinement statistics for HCoV-OC43 NP-NTD-H3 crystal.

crystal	HCoV-OC43 NP-NTD-H3
Data Collection	NSRRC BL13B1
Space group	P6 ₅
Resolution (Å)	30-2.50 (2.59-2.50) ^a
Wavelength (Å)	1.00000
Unit Cell Dimensions	
<i>a</i> = <i>b</i> (Å)	81.931
<i>c</i> (Å)	42.853
No. of reflections	
Observed	47726 (4777)
Unique	5733 (562)
Completeness (%)	98.7(100) ^a
<i>R</i> _{merge} (%)	2.4(4.4) ^a
<i>I</i> / σ (<i>I</i>)	83.1(48.3) ^a
Refinement	
No. of reflections	5707 (557)
<i>R</i> _{work} (95% data)	21.5 (24.8)
<i>R</i> _{free} (5% data)	26.9 (32.6)
Geometry deviations	
Bond lengths (Å)	0.017
Bond angles (°)	2.0
No. of all protein atoms	1100
Mean B-values (Å ²)	28.0
No. of ligand atoms	23
Mean B-values (Å ²)	52.1
No. of water molecules	37
Mean B-values (Å ²)	27.2
Ramachandran plot (%)	
Most favored	86.1
Additionally allowed	7.4
Other	6.5

^aValues in parentheses are for the highest resolution shells.

Reference

1. F. W. Denny and F. A. Loda, *The American journal of tropical medicine and hygiene*, 1986, 35, 1-2.
2. B. G. Williams, E. Gouws, C. Boschi-Pinto, J. Bryce and C. Dye, *The Lancet. Infectious diseases*, 2002, 2, 25-32.
3. B. D. Gessner, *Expert review of respiratory medicine*, 2011, 5, 459-463.
4. K. E. Arden, P. McErlean, M. D. Nissen, T. P. Sloots and I. M. Mackay, *Journal of medical virology*, 2006, 78, 1232-1240.
5. M. Owusu, A. Annan, V. M. Corman, R. Larbi, P. Anti, J. F. Drexler, O. Agbenyega, Y. Adu-Sarkodie and C. Drosten, *PloS one*, 2014, 9, e99782.
6. M. Venter, R. Lassauniere, T. L. Kresfelder, Y. Westerberg and A. Visser, *Journal of medical virology*, 2011, 83, 1458-1468.
7. H. Smuts, *Influenza and other respiratory viruses*, 2008, 2, 135-138.
8. H. Smuts, L. Workman and H. J. Zar, *Journal of medical virology*, 2008, 80, 906-912.
9. M. J. Adams and E. B. Carstens, *Archives of virology*, 2012, 157, 1411-1422.
10. A. Zumla, D. S. Hui and S. Perlman, *Lancet*, 2015, 386, 995-1007.
11. C. M. Coleman and M. B. Frieman, *Journal of virology*, 2014, 88, 5209-5212.
12. Z. Lou, Y. Sun and Z. Rao, *Trends in pharmacological sciences*, 2014, 35, 86-102.
13. S. Milne-Price, K. L. Miazgowicz and V. J. Munster, *Pathogens and disease*, 2014, 71, 121-136.
14. P. S. Masters, M. M. Parker, C. S. Ricard, C. Duchala, M. F. Frana, K. V. Holmes and L. S. Sturman, *Advances in experimental medicine and biology*, 1990, 276, 239-246.
15. Z. Hayouka, J. Rosenbluh, A. Levin, S. Loya, M. Lebendiker, D. Veprintsev, M. Kotler, A. Hizi, A. Loyter and A. Friedler, *Proceedings of the National Academy of Sciences of the United States of America*, 2007, 104, 8316-8321.
16. C. K. Chang, M. H. Hou, C. F. Chang, C. D. Hsiao and T. H. Huang, *Antiviral research*, 2014, 103, 39-50.
17. I. J. Chen, J. M. Yuann, Y. M. Chang, S. Y. Lin, J. Zhao, S. Perlman, Y. Y. Shen, T. H. Huang and M. H. Hou, *Biochimica et biophysica acta*, 2013, 1834, 1054-1062.
18. Y. Ma, X. Tong, X. Xu, X. Li, Z. Lou and Z. Rao, *Protein & cell*, 2010, 1, 688-697.
19. K. S. Saikatendu, J. S. Joseph, V. Subramanian, B. W. Neuman, M. J. Buchmeier, R. C. Stevens and P. Kuhn, *Journal of virology*, 2007, 81, 3913-3921.
20. H. Jayaram, H. Fan, B. R. Bowman, A. Ooi, J. Jayaram, E. W. Collisson, J. Lescar and B. V. Prasad, *Journal of virology*, 2006, 80, 6612-6620.
21. I. M. Yu, M. L. Oldham, J. Zhang and J. Chen, *The Journal of biological chemistry*, 2006, 281, 17134-17139.
22. H. Fan, A. Ooi, Y. W. Tan, S. Wang, S. Fang, D. X. Liu and J. Lescar, *Structure*, 2005, 13, 1859-1868.
23. Y. S. Wang, C. K. Chang and M. H. Hou, *Acta crystallographica. Section F, Structural biology communications*, 2015, 71, 977-980.
24. N. E. Grosseohme, L. Li, S. C. Keane, P. Liu, C. E. Dann, 3rd, J. L. Leibowitz and D. P. Giedroc, *Journal of molecular biology*, 2009, 394, 544-557.
25. Q. Huang, L. Yu, A. M. Petros, A. Gunasekera, Z. Liu, N. Xu, P. Hajduk, J. Mack, S. W. Fesik and E. T. Olejniczak, *Biochemistry*, 2004, 43, 6059-6063.
26. S. Chenavas, T. Crepin, B. Delmas, R. W. Ruigrok and A. Slama-Schwok, *Future microbiology*, 2013, 8, 1537-1545.

27. Y. S. Lo, S. Y. Lin, S. M. Wang, C. T. Wang, Y. L. Chiu, T. H. Huang and M. H. Hou, *FEBS letters*, 2013, 587, 120-127.
28. S. Y. Lin, C. L. Liu, Y. M. Chang, J. Zhao, S. Perlman and M. H. Hou, *Journal of medicinal chemistry*, 2014, 57, 2247-2257.
29. L. Pu, A. A. Amoscato, M. E. Bier and J. S. Lazo, *The Journal of biological chemistry*, 2002, 277, 46877-46885.
30. J. S. Lazo, D. C. Aslan, E. C. Southwick, K. A. Cooley, A. P. Ducruet, B. Joo, A. Vogt and P. Wipf, *Journal of medicinal chemistry*, 2001, 44, 4042-4049.
31. Y. S. Lo, W. H. Tseng, C. Y. Chuang and M. H. Hou, *Nucleic acids research*, 2013, 41, 4284-4294.
32. H. C. Hung, C. L. Liu, J. T. Hsu, J. T. Horng, M. Y. Fang, S. Y. Wu, S. H. Ueng, M. Y. Wang, C. W. Yaw and M. H. Hou, *Analytical chemistry*, 2012, 84, 6391-6399.
33. C. K. Chang, Y. L. Hsu, Y. H. Chang, F. A. Chao, M. C. Wu, Y. S. Huang, C. K. Hu and T. H. Huang, *Journal of virology*, 2009, 83, 2255-2264.
34. C. Y. Huang, Y. L. Hsu, W. L. Chiang and M. H. Hou, *Protein science : a publication of the Protein Society*, 2009, 18, 2209-2218.

Figure 2

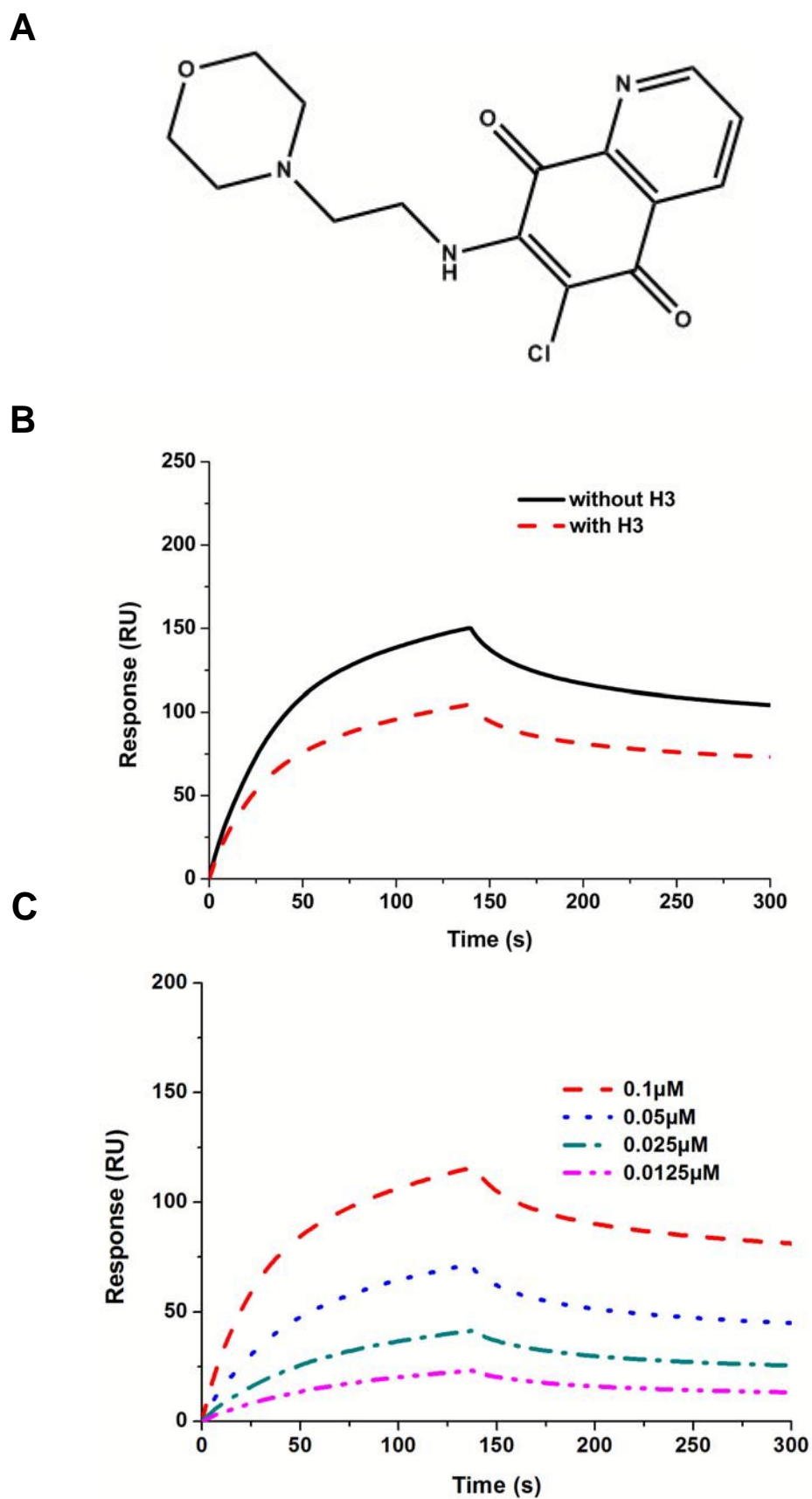


Figure 3

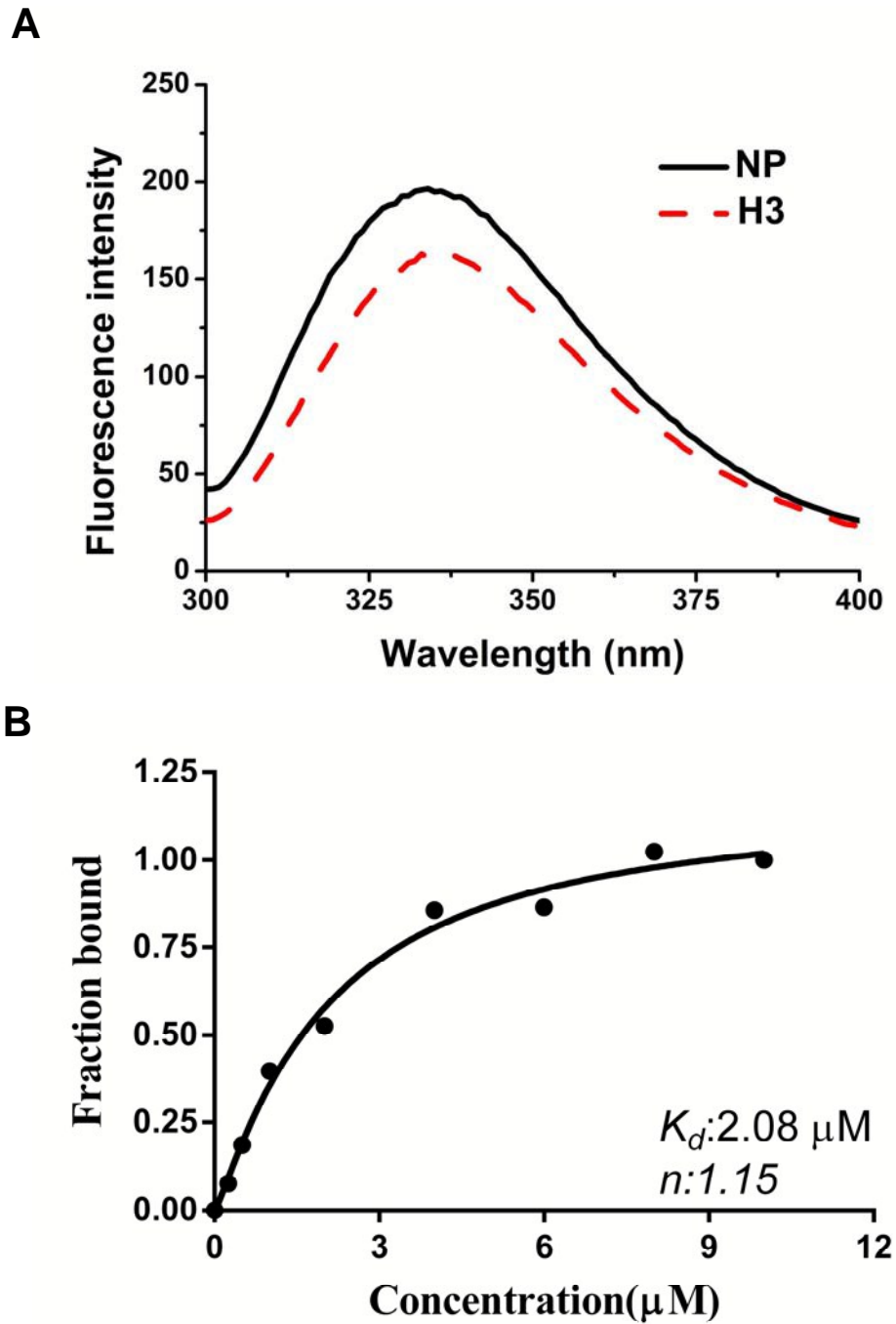


Figure 4

